Journal of Mechanics Engineering and Automation 2 (2012) 256-266

Swirl Jets in Crossflow at Low Velocity Ratios

Alexandros Terzis[1], Charilaos Kazakos[2], Anestis I. Kalfas[2], Pavlos K. Zachos[3] and Peter Ott[1]

1. Group of Thermal Turbomachinery, EPFL-SCI-STI-PO, Swiss Federal Institute of Technology, Lausanne CH-1015, Switzerland

2. School of Engineering, Aristotle University of Thessaloniki, Thessaloniki GR-54-124, Greece

3. Department of Power and Propulsion, Cranfield University, Bedfordshire MK43 0AL, UK

Received: February 11, 2012 / Accepted: February 24, 2012 / Published: April 25, 2012.

Abstract: This investigation examines experimentally the behavior of swirled jets produced by axial flow fans blowing into a crossflow at low velocity ratios. The main difference with non-swirl cases is an asymmetry of the dominant kidney vortex and a slight distortion of the jet trace downstream of the injection hole. The effect of jet rotation at relatively low swirl numbers and similar velocity ratios is also investigated by a validated computational analysis tool. The numerical results are analyzed by means of various post-processing procedures, aiming to clarify, quantify and analyze the impact of swirl on the characteristics and the flow domain of a jet in crossflow. In general, swirl introduces an asymmetry in all examined quantities and prevents the penetration of the jet into the crossflow, causing the jet to remain closer to the wall surface. The rotation of the injected fluid results in an imparity of the two parts of the Counter Rotating Vortex Pair (CVP) which is no longer symmetric to the axial centerline plane. High swirl numbers result in the destruction of the CVP and the dominant kidney shape vortex is transformed into a comma shape vortex, rotating close to the wall.

Key words: Jet in crossflow, swirl, CFD (computational fluid dynamics).

Nomenclature

x, y, z	coordinates in streamwise, spanwise and normal to the wall direction, respectively
d	jet diameter
R	jet radius = $d/2$
V	velocity
G	momentum flux
r	velocity ratio
$y+$	non-dimensional wall distance
S	swirl number

Greek

θ	tangential direction
Ω	angular velocity
ω	streamwise vorticity
ρ	density

Subscripts

j	jet
cf	crossflow
m	average value
o	maximum value

Corresponding author: Alexandros Terzis, researcher, research field: gas turbine heat transfer. E-mail: alexandros.terzis@epfl.ch.

1. Introduction

Jets In CrossFlow (JICF) are used in a variety of engineering applications. Depending on the jet to cross-stream blowing ratio the resulting flow field can be found in the mixing and dispersion of emitted gases from chimneystacks, in fuel injectors, in Vertical/Short Take-off and Landing aircrafts (V/STOL) as well as in cooling of turbine blades. The main parameter used to describe a jet in crossflow is the velocity ratio, r, which is simplified for incompressible flows as follows:

$$r = \left(\frac{\rho_j {V_{z,j}}^2}{\rho_{cf} {V_{x,cf}}^2}\right)^{1/2} \xrightarrow{\rho_j=\rho_{cf}} r = \frac{V_{z,j}}{V_{x,cf}} \quad (1)$$

The practical importance of JICF led to an extensive amount of experimental investigations, where a detailed review can be found in Ref. [1]. In the beginning of JICF research, particular emphasis was given on the structure of transverse jets focusing on the jet trajectory and spreading as well as on the mean velocity field downstream of the jet for various velocity ratios. Authors of Refs. [2-4] concluded that the jet

penetrates further into the crossflow as the velocity ratio increases, while the bending-over of the jet takes place more gradually at higher velocity ratio values. On the other hand, when the momentum of the jet is lower than the momentum of the crossflow ($r < 1$) abrupt jet inflection is unavoidable and the trajectory of the jet remains closer to the wall surface. Turbulence characteristics of a normal round jet in crossflow reported by Andreopoulos and Rodi [5], Sherif and Pletcher [6] and Kim et al. [7] who observed a great dependence of turbulent kinetic energy with the velocity ratio while more recent studies ([8-13]) established that the resulting flow field is quite complex and characterized by a spectrum of vortical structures including the dominant kidney vortex, also known as Counter rotating Vortex Pair (CVP), the horseshoe vortex, the wake vortex and the shear layer vortices. Moreover, a lot of experimental studies investigated the film cooling of turbine blades using a normal jet injected in freestream flow [14-17]. The main conclusion is that higher thermal protection is achieved at lower momentum or velocity ratios. Lower momentum of the jet results in lower energy of the CVP, which is unable to lift-off from the blade surface and remains closer to the wall creating a protective film layer. New et al. [18] investigated the structure of an elliptic JICF and reported a strong dependence on the aspect ratio of the nozzle exit, while Jovanovic et al. [19] focused on the influence of shaped holes and imperfect geometry. Hu [20], observed increased values of film cooling effectiveness at higher blowing angles, while Brauckmann et al. [21] and Aga et al. [22] have demonstrated improvements on the thermal protection, using cooling holes with expanded exits (compound angle) aiming at reducing the momentum of the jet as well as aligning the film cooling traces on the blade.

The effect of many geometrical and numerical parameters on the structure of straight round JICF is well documented in the literature. However, the number of investigations focused on Swirl Jets in Crossflow (SJICF) is limited in the open literature and the majority of them are experimental. Kavsaoglou and Schetz [23] investigated low swirl numbers at velocity ratios between $r = 2.2 \sim 8$ and observed an asymmetry on the surface pressure distribution with increasing swirl number and a reduced penetration distance into the crossflow. Liscinsky et al. [24], at $r = 8.5$, reported that swirl jets prevent the development of the CVP and induce a distortion of the jet trace. Similar conclusions, obtained from experiments in water-tunnels, were reported by Niederhaus et al. [25] and Yingjaroen et al. [26]. The swirl number in these investigations was varied from 0.08 to 0.17 and 0.5 to 0.8, respectively. Niederhaus et al. [25] observed an asymmetry of the CVP with the degree of asymmetry been increased with the swirl number, while Yingjaroen et al. [26] reported a bias of the jet trace at $r = 3.8$. Yoshizako et al. [27], at $r = 4$ and high swirl numbers found an acceleration of the crossflow at the side of the injection hole where the velocity of the jet is in the same direction with the crossflow. Kraus and Culter [28] and Culter and Doerner [29] investigated supersonic swirl jets discharged into a crossflow. Both investigations concluded that swirl slightly reduces the penetration of the jet while the former work reported also a lateral displacement downstream of the injection hole. Regarding heat transfer rates, Bunyajitradulya and Sathapornnanon [30] presented some preliminarily findings on the temperature distribution of a SJICF, at a constant swirl number of 0.52. However, conclusions for film cooling applications are not possible due to the high velocity ratio, $r = 4$.

The velocity ratio considered in the above discussed investigations varies between 2.2 and 8.5, far away from the typical values used in the cooling of turbine blades ($r \sim 1$). The main objective of the present investigation is to enhance the current knowledge on swirl jets in crossflow and study their behavior at velocity ratios typically used for film cooling applications. First, the effect of velocity ratio on swirl jets, produced by axial flow fans in crossflow, is

investigated experimentally indicating the similarities with non-swirled situations. In addition, the impact of swirl on the average flow field is analyzed using a computational tool validated with the results of previous authors. The numerical results are post-processed in order to clarify and qualify the impact of swirl on the interaction between the jet and the crossflow.

Parts of this work are published by 9th European Conference on Turbomachinery, Istanbul, Turkey, March 21-25, 2011.

2. Experimental Setup and Procedure

In general, there are three principal methods for generating swirl flow in pipes or nozzles. Kavsaoglou and Schetz [23] used tangential entry slots in their jet pipe in order to produce fluid flow in the tangential direction, while Liscinsky et al. [24] generated variable swirl numbers by adjusting the position of guide vanes (stator blades at different angles) installed just upstream of the nozzle exit. The use of direct rotation of a pipe is another successfully technique of swirl production used in the flow visualization experiments of Yingjaroen et al. [26]. However, this study produces swirl by axial flow fans blowing into a crossflow similar to Niederhaus et al. [25] who used a four-bladed paddle mounted on the shaft of a stepper motor used for the rotation of the paddle. The drawback of this method is the unique swirl number produced by the fan impeller.

The experiments were carried out in the closed-loop wind tunnel of Aristotle University of Thessaloniki, Greece. The test section consists of a rectangular flow path of 600 × 600 mm^2 cross-section and 1200 mm length. Swirl flow and periodicity were investigated by a cascade of three fan configurations embedded into the test surface 7D downstream of the leading edge of the plate where the fans were mounted in order to allow reattachment and laminar approaching boundary layer profile, validated by oil and dye flow visualization. The exit of the fans is located directly down of the plate. The cascade pitch was three fan diameters. Three jets were thereby produced by twin stage axial flow fans where their performance is described in more details in Terzis et al. [31]. The Reynolds number of the crossflow based on jet diameter was varied between 3 × 10^4 and 5 × 10^4. Typical mainstream turbulence intensity values are in the order of 1.5%.

At the top of the test section of the wind tunnel, a simple traversing probe access technique, similar to the circle-in-circle system presented by Aga et al. [22] is used to perform the pneumatic probe measurements. The main advantage of this traversing wall mechanism is the ease in manufacturing and the absolute flexibility in spatial access. The movement of the probe is achieved using small size and high performance stepping motor controllers in order to achieve increased accuracy regarding the probe movement. A calibrated 5-hole probe with a cobra-style head was used for the measurements presented in this study. The probe tip diameter is 2.65 mm and the internal diameter of each hole is 0.254 mm. The measurements were performed at four different planes upstream and downstream of the cross section of the fans and perpendicular to the primary free stream velocity as shown in Fig. 1 (x/d = −0.5, 0.5, 1.5, 3). Each normal plane consisted of 86 wall lateral and 46 wall normal nodes, composing a mesh of 3956 measurement points. Owing to the size of the probe tip, the closest to the wall point of measurement was approximately 5mm (z/d = 6.5%). Pressure signals were acquired using a self-contained 16-channel high performance pressure acquisition module. The pressure scanner has the capability to

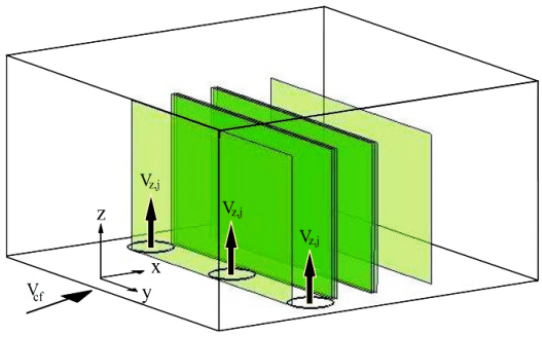

Fig. 1 Schematic of the test section.

sample, at rates up to 100 measurements per second, while the sensor zero drift error is eliminated, resulting in a system accuracy of up to ± 0.05% after rezeroing.

3. Computational Analysis Tool and Physical Implementation

Accurate predictions of JICF have been difficult to obtain due to the complexity of the flow. Subsequently, various numerical models have been used in the past and their applicability in JICF flow applications can be found in the studies of Amer et al. [32], Sarkar and Bose [33]. Reynolds-averaged equations models (RANS), used by Chochua et al. [34] and Pathak et al. [35], were found to predict well the trajectory and the jet exit velocity profile while under-predicting the spreading of the jet and the mixing with the crossflow. Other authors used Large-Eddy-Simulation (LES) (Yuan et al. [36], Schluter and Schonfeld [37]) and observed good agreement with experiments while Muppidi and Mahesh [38] and Muldoon and Acharya [39] used Direct Numerical Simulation (DNS) tools to obtain the coherent structures at the jet wake. In general, two-equation turbulent models found to over-predict the penetration distance and under predict the spreading of the jet. The drawbacks of RANS models on unsteady flow fields have been discussed by Acharya et al. [40]; however, two equation models are extensively employed as an industrial design tool for film cooling flows due to the high computational cost of LES and DNS. Several standard turbulence models were applied to perform the non-swirl and swirl jet in crossflow RANS simulations, but only the Shear Stress Transport (SST), k-ω model provided acceptable results. In addition, many authors reported the good behavior of k-ω, in adverse pressure gradients and separating flows. The solution of the non-conservative steady Navier-Stokes equations in their incompressible form is achieved using a coupled implicit steady solver (FLUENT 6.3). For the purposes of this study, a hybrid mesh was used, consisting of an O-type, structured mesh around the jet exit and an unstructured mesh in the rest of the control volume. The mesh contained approximately 0.5 M cells, the majority of them located directly downstream of the injection hole. In addition, the trial and error method used to thicken the mesh along the jet trajectory while typical cell sizes near the wall were selected in order to give values of $y+ < 5$. All computations were performed with the same numerical grid while the convergence criterion is that the residual of each calculated parameter is less than 10^{-7}.

The principal computational domain is shown in Fig. 2; $z = 0$ plane, represents the wall surface while the origin of the coordinate system was located at the center point of jet exit and placed 7D downstream of the inlet plane. The total length of the control volume is 20 D while a rectangle cross section was used with side dimension of 7D. The round jet exit does not extend downward ($z < 0$) of the control volume provided a top-hat velocity profile at the injection hole. This configuration corresponds to an experiment where an axial swirl generator is placed directly at the jet exit. Periodic boundaries were imposed on the side walls in order to investigate possible interactions between two adjacent holes at high swirl numbers while the exit of the computational domain was treated as pressure outlet. Swirl number is defined as the ratio of axial flux of angular momentum divided by the axial flux of axial momentum times the equivalent jet radius. According to the coordinate system used in this study, the following simplified expression can be obtained for the definition of swirl number:

$$S = \frac{G_\theta}{G_z R} = \frac{1}{R}\frac{\int_0^{R_o} \rho V_z V_\theta R^2 dR}{\int_0^{R_o} \rho V_Z^2 R dR} \quad (2)$$

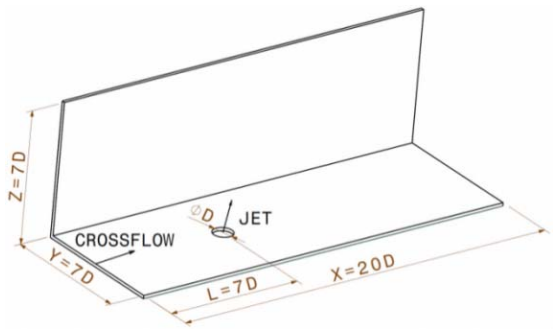

Fig. 2 Sketch of the computational domain.

Comparison between the experimental results and the various options in the vortex design has revealed that the solid vortex design was the most appropriate choice for the representation of the swirl jet. The solid vortex design describes more appropriately the experimental setups of previous authors as well as the test rig of this study where the jets are generated by low solidity fans. Therefore, a forced vortex principal was selected, where jet fluid rotates as a solid body without shear stresses. This motion can be realized by placing the jet on a turntable rotational speed, Ω. This result in a constant axial velocity profile and a continuous increasing tangential velocity from 0 ($R = 0$) to V_θ, max ($R = R_o$):

$$\mathrm{V_{z,j}(R) = V_z} \quad / \ \mathrm{V_{\theta,j}(R) = \Omega R} \tag{3}$$

The assumption of a solid body rotation plug flow results in a deduction of Eq. (2). Substitution of the above equations in Eq. (2) and integration, results in a simplified formula for the swirl number which can be written as

$$\mathrm{S = \frac{\Omega R_o}{2}\frac{1}{V_{z,j}}} \tag{4}$$

This means that S is equal to the half magnitude of the tangential velocity at the vortex tip (average swirl velocity) divided by the axial (normal to the jet exit) velocity component. However, it should be noted that in real swirling flows the tangential velocity distribution is intermediate between forced vortex and free vortex flow (Rankine vortex).

4. Numerical Model Validation

Previous experimental works focused on SJICF are not suitable for validation purposes due to their restriction to flow visualization, surface contours and some supersonic cases. Therefore, the validation of the computational tool is limited to straight jets, $S = 0$ and the results of Niederhaus et al. [25] who presented the effect of swirl on the jet trajectory. The jet trajectory can be defined by various ways, however, in this study the streamline from the center of the jet exit is considered. Estimation of jet trajectories has been suggested by many analytical models [2, 41-42]; however, the velocity ratio multiplied by the jet diameter is a quite acceptable length scale used to allow comparisons of JICF at different Reynolds numbers. Fig. 3a indicates the trajectory of the jet for the case without swirl scaled by, rd. Good agreement between the predicted CFD trajectory and the experimental data is observed over the entire range of velocity ratios. Note also the abrupt inflection of the jet at the low velocity ratios used in this study as well as the general trend of increasing penetration depth with increasing r. Fig. 3a contains also results of more complex numerical tools (LES-DNS), indicating that the jet trajectory obtained from the average flow fields of unsteady computations is not far from RANS. The validation of jet trajectory in swirl cases ($S > 0$) was based on the experimental investigation of Niederhaus et al. [25], who used planar laser-induced fluorescence in a water tunnel, to measure the mean concentration field downstream of the jet. Fig. 3b indicates that the numerical model predicts also quite well the inflection of the jet at swirl inlet conditions.

In addition, Fig. 4 indicates reasonably good agreement in the longitudinal mean velocity profiles at various downstream positions ($x/d = -0.5$, 0, 2 and 4), compared to the experimental data of Andreopoulos and Rodi [5], for $r = 0.5$. A deceleration of the crossflow is observed due to the impact with the jet ($x/d = -0.5$), however, over the injection hole the freestream fluid causes an inflection and acceleration to the jet so that the velocity of the inflected jet is slightly higher than the crossflow velocity, V_{cf}. In general, the use of an isotropic eddy-viscosity model in a highly anisotropic and unsteady region of a jet-crossflow interaction introduces lack of similarities between the experimental data and the results of the numerical model very close to the wall. However, as a general conclusion, it can be stated that RANS approach provides acceptable predictions on the mean flow quantities and is still an appropriate methodology, considering also the low CPU costs.

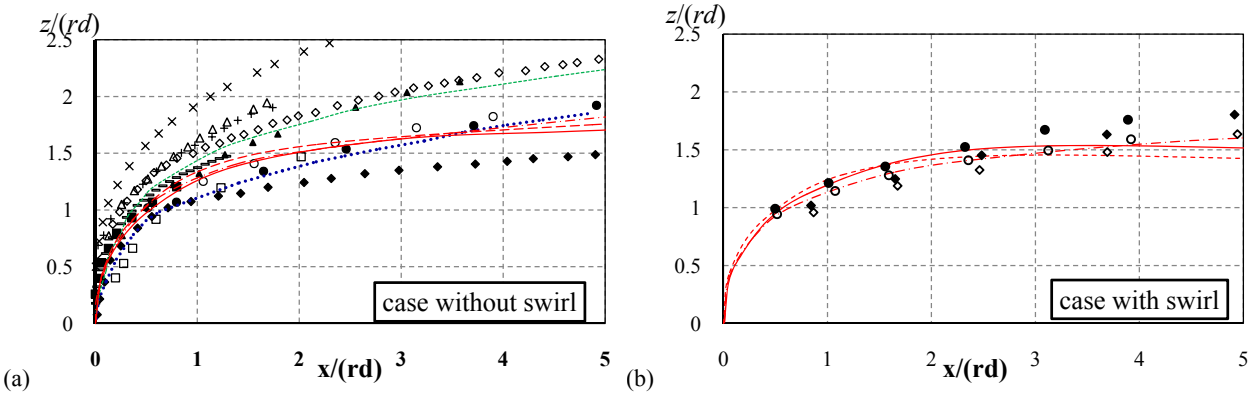

Fig. 3 Comparison of scaled jet trajectories using (a) straight jets in crossflow: ■/*r* = 2, □/*r* = 4 [2], ▲/*r* = 3.9, Δ/*r* = 7.7 [3], ●/*r* = 4.9, ○- *r* = 7.9 [25], ♦/*r* = 5, ◊/*r* = 10 [43], +/*r* = 5.81 [34], —/*r* = 3.3 [7], *x*/*r* = 5.7 [44], •••/*r* = 2/LES [36], ---/*r* = 1.52/DNS [38], —/*r* = 0.8 , −−−/*r* = 1, – • –/*r* = 1.3, k-ω, this study; (b) swirled jets in crossflow: ♦/*r* = 4.9, *S* = 0.13, ◊/*r* = 7.7, *S* = 0.17, ●/*r* = 4.9, *S* = 0.13, ○- *r* = 7.9, *S* = 0.17 [25], —/*r* = 0.8, −−−/*r* = 1, – • –/*r* = 1.3, k-ω, this study *S* = 0.2.

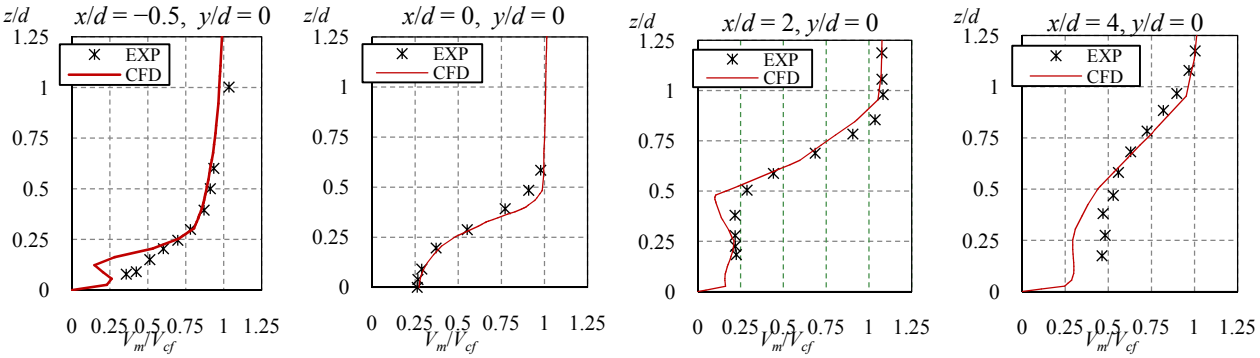

Fig. 4 Velocity profiles at various positions. Exp. data: Ref. [5].

5. Experimental Results—Isosurface

Fig. 5 illustrates the effect of the velocity ratio on the penetration and the flow domain of a swirl jet (fan) into a transversal moving stream (crossflow). In these series of experiments, the velocity of the crossflow was varied, with constant jet axial (normal to the crossflow) velocity, in order to achieve the required velocity ratios of 0.75, 1.00 and 1.25. The results show that the flow field at the jet exit is highly affected by the momentum of the crossflow. Although a reasonable amount of rotation (swirl) was induced in the jet by the rotor of the fans, Fig. 5 indicates good agreement with the general trend obtained by straight jets in crossflow in the open literature. The jet penetrates further into the crossflow as the velocity ratio increases, however, a large asymmetry of the flow domain can be observed due to the induction of swirl. An imparity between the two parts of the counter rotating vortex pair can be observed, due to the rotation of the jet. This difference is more visible at $r = 1$ where the right part of the kidney vortex is apparently bigger than the left part. In addition, at $r = 1.25$ a diversion of the jet trace is observed in agreement with the lateral displacement as observed by Kraus and Culter [28] and Yingjaroen et al. [26].

6. Influence of Swirl on the Flow Domain

6.1 Jet Trajectory

The trajectory of a jet in crossflow is a primary characteristic of interest and as discussed earlier many analytical models have been suggested for its estimation. The main objective of this section is to study the effect of swirl number, *S*, on the jet trajectory. This section scales the trajectory only with the jet diameter,

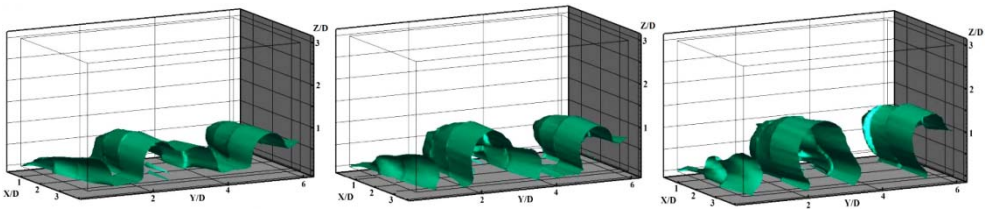

(a) Swirl jet trace, $r = 0.75$ (b) Swirl jet trace, $r = 1$ (c) Swirl jet trace, $r = 1.25$

Fig. 5 Total pressure charts.

d, in order to allow comparisons for the penetration distance of the jet into the crossflow at different velocity ratios. Note again that jet trajectory is defined as the center streamline at the jet exit. Fig. 6 indicates deeper penetration of the jet as the velocity ratio increases from $r = 0.8$ to $r = 1.3$. In addition, a noticeable effect of swirl is observed in all studied cases. At these velocity ratios, even if a small amount of swirl is added ($S = 0.1$), the penetration depth is slightly decreased relative to the non-swirl condition.

6.2 Surface Pressure Distribution

Fig.7 illustrates the static pressure distribution at the wall ($z/d = 0$) for $r = 1$, at various swirl numbers. For $S = 0$, the distribution of static pressure is symmetrical along the streamwise centerline, however, this distribution is distorted with increasing swirl. In particular, the magnitude of static pressure is attenuated on one side ($y/d < 0$) and enhanced on the other side ($y/d > 0$). The degree of asymmetry is increased with increasing swirl number in agreement with the preliminarily experimental findings of Kavsaoglou and Schetz [23]. According to the aerodynamics of Magnus effect, suction side can be referred to the lateral side of the jet where the tangential velocity is in the same direction with the crossflow while pressure side the opposite. The asymmetry of the static pressure distribution is due to the increased lateral shear between the jet fluid and the crossflow on the suction side and a corresponding reduction in the shear on the opposite side. As a result, at the suction side ($y < 0$) the fluid is accelerated and results in negative pressure gradients while increased values of static pressure appear on the pressure side ($y > 0$).

6.3 Flow Streamlines

Fig. 8 indicates flow streamlines at $x/d = 2.5$ and perpendicular to the crossflow direction. For S = 0, the streamlines are symmetrical indicating that the CVP is developed similarly on both lateral sides of the jet. In addition, the penetration of the jet is obviously lower at $r = 0.8$ than at $r = 1.3$. At higher swirl numbers ($S = 0.2$), the rotation results in an asymmetry of the CVP where the left part of the kidney vortex becomes smaller (with increased strength) while its companion vortex of the CVP is attenuated in strength due to the increased size. Further increase of swirl ($S = 0.4$) destroys and prevents the development of the CVP where the dominant kidney shape vortex is transformed into a comma shape vortex. Moreover, Fig. 8 provides information on how the jet approaches the wall with increasing swirl. Comparing the streamline patterns for $S = 0$ and $S = 0.2$, a reduced height of the left vortex of the CVP is observed while the mutual vortex remains approximately at the same vertical distance. Obviously, the overall penetration depth is reduced with increasing swirl. This is in agreement with the preliminarily findings of some experimental works at higher velocity ratios [23-25].

6.4 Vorticity

Fig. 9 illustrates the streamwise vorticity component (ω_x) at two different swirl numbers ($S = 0.2$ and 0.4) when the axial momentum of the jet equals the momentum of the crossflow ($r = 1$). The vorticity contours are normalized by the maximum values appeared in the planes while the vorticity spots are located close to the wall in the region of wake vortices.

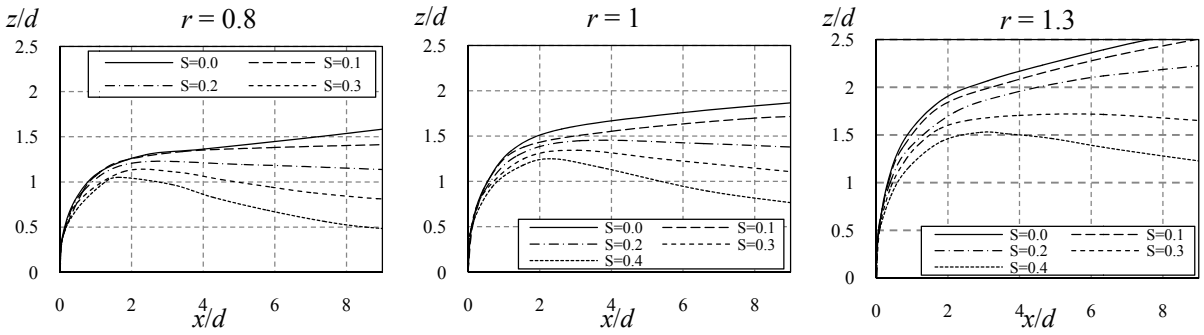

Fig. 6 Penetration depth at various swirl numbers.

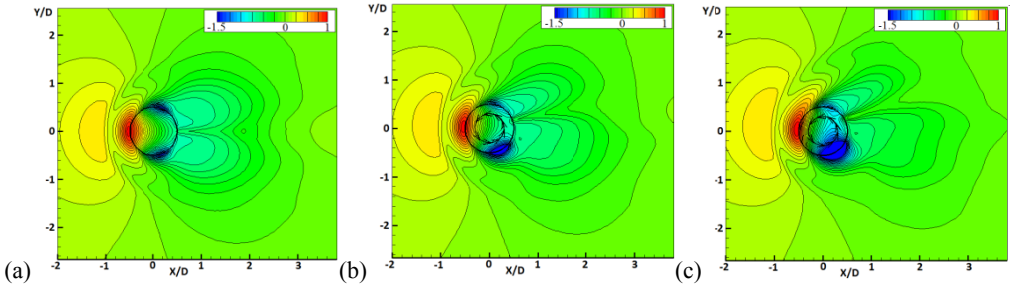

Fig. 7 Surface static pressure distribution of at various swirl numbers.

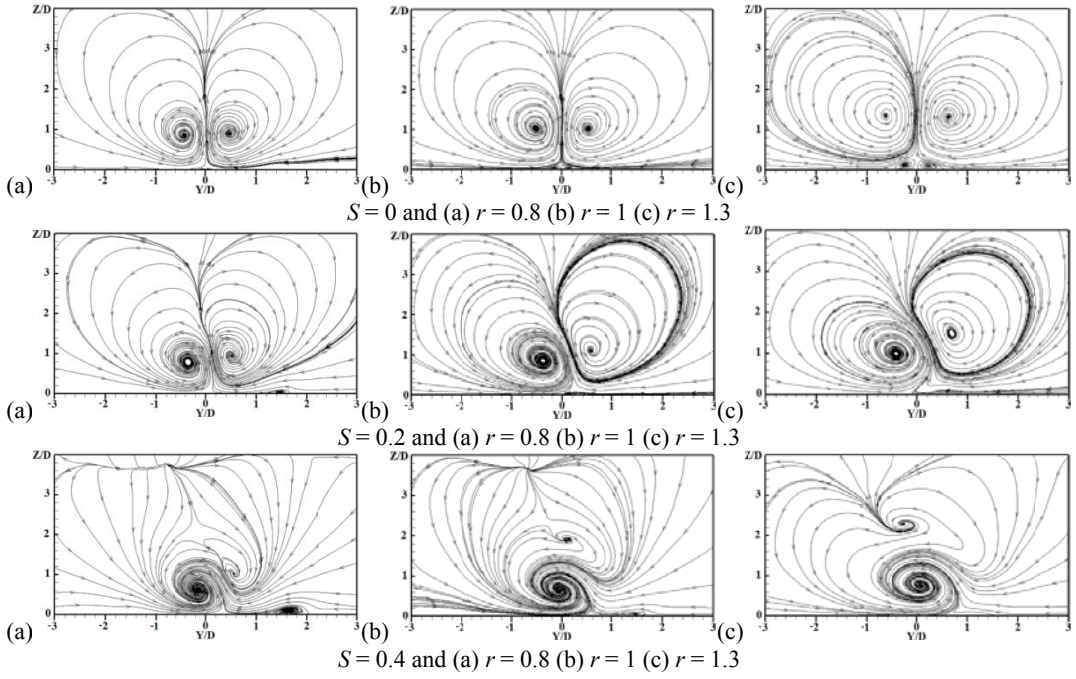

$S = 0$ and (a) $r = 0.8$ (b) $r = 1$ (c) $r = 1.3$

$S = 0.2$ and (a) $r = 0.8$ (b) $r = 1$ (c) $r = 1.3$

$S = 0.4$ and (a) $r = 0.8$ (b) $r = 1$ (c) $r = 1.3$

Fig. 8 Flow streamlines at $x/d = 2.5$ and $r = 0.8 \sim 1.3$ for various swirl numbers.

In all cases, the vorticity maximum point inside the CVP is observed closer to the centerplane. This is generated by the upward moving shear layer entrained into the interior of the jet. Fig. 9 shows that swirl velocity induced in the jet prevents the penetration of the jet fluid into the crossflow. Although at $X/D = 2.5$ downstream of the jet, the location of the CVP for the three cases appears approximately at the same height, further downstream in the streamwise direction ($X/D = 7.5$) the jet without swirl gains more height during the evolution of the phenomenon while in the cases with swirl the jet remains closer to the wall.

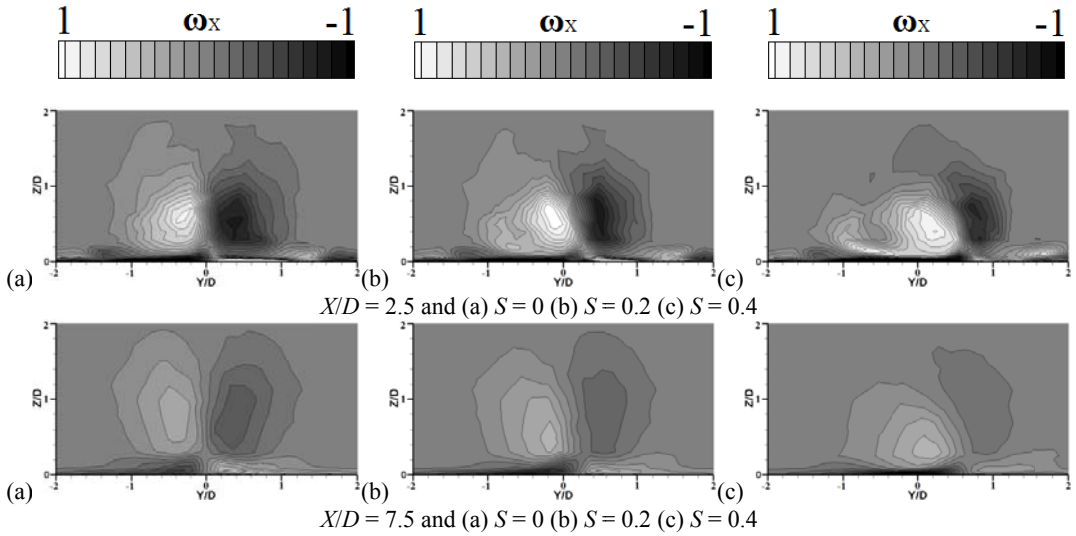

Fig. 9 Vorticity contours at X/D = 2.5 and 7.5 for S = 0, 0.2 and 0.4 (r = 1).

The rotation of jet introduces also an asymmetry of the flow domain with the degree of asymmetry increasing with the swirl number. The asymmetry of the CVP is more evident at smaller distances downstream of the jet (X/D = 2.5). As the rotation of the jet increases the left vortex of the CVP is enhanced while the companion vortex of the CVP is attenuated. Therefore, the region of high vorticity values of the left vortex of the CVP becomes substantially broader. It is evident that the rotation of the jet prevents also the development of the kidney vortex, which is the main characteristic of this phenomenon.

In addition, due to the rotation of the jet, the injected fluid obtains a positive vorticity in the y-direction and subsequently not only bends in the direction of the crossflow but also diverts in the direction of the rotation, in order to maintain its angular momentum. The left part of the vortex is shifted in the centerline of the plane (y/d = 0), indicating a small bias of the jet trace The bias of the jet trace is more evident at a certain distance downstream of the cross section of the jet (that is X/D = 7.5, Fig. 9).

7. Conclusions

This investigation presents the results of an experimental and numerical approach of a swirling transverse jet entering into a crossflow, at low momentum ratios (r = 0.75 ~ 1.3). The main objective of this work was to examine the flow domain and the characteristics of a swirled jet in crossflow (JICF) at incompressible conditions.

In agreement with straight (non-swirled, S = 0) jets in crossflow, the experimental data indicated that swirled jets penetrate further into the crossflow with increasing velocity ratio r while better interaction between adjacent jets is achieved at the lowest velocity ratio (r = 0.75) resulting in a broader protective film layer.

The effect of swirl velocity at a given momentum ratio was investigated using a computational analysis tool validated with the results of previous investigations focused on straight and swirled jets in crossflow. The effect of swirl was found to be fairly complex and roughly independent on the range of velocity ratios used in this study. The induction of swirl results in a general asymmetry all of the quantities examined, while the degree of asymmetry is increased as the swirl number increases. The findings of this investigation can be summarized as follows:

- An asymmetry of the wall static pressure distribution was found when swirl was induced at the inlet conditions of the jet exit. The degree of asymmetry increases with increasing swirl number;
- Swirl velocity reduces the penetration distance

compared with the case without swirl while the reduction of the height is highly dependent on the proportion of added swirl and the velocity ratio. In particular, the higher value of swirl number and velocity ratio, the higher reduction of penetration height. This can be attributed to the attenuation (or destruction) of the CVP which is unable to lift-off the jet from the surface;

- Swirl velocity attenuates the effect of velocity ratio on the penetration depth;
- When the added swirl exceeds a critical swirl number, the trajectory of the jet approaches the wall shortly downstream of the injection hole. The critical swirl number was about $S = 0.2$ from $r = 0.8$ to $r = 1$ and $S = 0.3$ for the highest velocity ratio ($r = 1.3$);
- The rotation of the injected fluid results in an imparity of the two parts of the CVP which is no longer symmetrical to axial centerline. The size of the vortex part whose tangential velocity is in the same direction with the crossflow is reduced compared with its contra rotating pair while the center of the vortex rotation approaches the wall;
- High swirl numbers, $S = 0.4$, result in a destruction of the CVP and the dominant kidney shape vortex is transformed into a comma shape vortex, rotating very close to the wall;
- Jet rotation results also in a bias of the jet trace similar to the aerodynamics of Magnus effect.

Acknowledgments

The authors would like to acknowledge Dr. Christos Frouzakis and Dr. Christos Altantzis for their overall contribution.

References

[1] R.J. Margason, Fifty years of jet in cross flow research, in: Proceedings of the AGARD Symposium on Computational and Experimental Assessment of Jets in Crossflow, UK, 1993, AGARD-CP-534.

[2] J.R. Keffer, W.D. Baines, The round turbulent jet in a cross-wind, Journal of Fluid Mechanics 15 (1963) 481-496.

[3] Y. Kamotani, I. Greber, Experiments and turbulent jet in crossflow, AIAA Journal 10 (1972) 1425-1429.

[4] D. Crabb, D.F. Durao, J.H. Whitelaw, A round jet normal to a crossflow, Journal of Fluids Engineering, AMSE 103 (1981) 142-151.

[5] J. Andreopoulos, On the structure of jets in crossflow, Journal of Fluid Mechanics 105 (1985) 163-197.

[6] J. Andreopoulos, W. Rodi, Experimental investigation of jets in crossflow, Journal of Fluid Mechanics 138 (1985) 93-127.

[7] S.A. Sherif, R.H. Pletcher, Measurements of the flow and turbulence characteristics of round jets in crossflow, Journal of Fluids Engineering 111 (1989) 165-171.

[8] K.C. Kim, S.K. Kim, S.Y. Yoon, PIV measurements of the flow and turbulent characteristics of a round jet in crossflow, Journal of Visualization 3 (2) (2000) 157-164.

[9] T.F. Fric, A. Roshko, Vortical structure in the wake of a transverse jet, Journal of Fluid Mechanics 279 (1994) 1-47.

[10] R.M. Kelso, A.J. Smits, Horseshoe vortex systems resulting from the interaction between a laminar boundary layer and a transverse jet, Physics of Fluids 7 (1995) 153-158.

[11] R.M. Kelso, T.T. Lim, A.E. Perry, An experimental study of round jets in crossflow, Journal of Fluid Mechanics 306 (1996) 111-144.

[12] L. Cortelezzi, A.R. Karagiozian, On the formation of the counter-rotating vortex pair in transeverse jets, Journal of Fluid Mechanics 446 (2001) 347-373.

[13] S. Gopalan, B.M. Abraham, J. Katz, The structure of a jet in crossflow at low velocity ratios, Physics of Fluids 16 (6) (2004) 2067-2087.

[14] L. Su, M.G. Mungal, Simultaneous measurements of scalar and velocity field evolution in turbulent crossflowing jets, Journal of Fluid Mechanics 513 (2004) 1-45.

[15] G. Bergeles, A.D. Gosman, B.E. Launder, The near-field character of a jet discharged through a wall at 90 deg. to a main stream, ASME Paper 75-WA/HT-108, 1976.

[16] R.J. Goldstein, T. Yoshiba, The influence of laminar boundary layer and laminar injection on film cooling performance, Journal of Heat Transfer 104 (2) (1982) 355-362.

[17] D. Bohn, K. Karsten, Influence of blowing ratio on cooling efficiency of lateral leading edge ejection, in: ISABE, Paper No. ISABE99-7200, Florance, Italy, Sep. 5-10, 1999.

[18] T.H. New, T.T. Lim, S.C. Luo, Elliptic jets in crossflow, Journal of Fluid Mechanics 494 (2003) 119-140.

[19] M.B. Jovanovic, H.C. de Lange, A.A. van Steenhoven, Influence of hole imperfection on jet in crossflow, Int. Journal of Heat and Fluid Flow 27 (2006) 42-53.

[20] Y. Hu, H. Ji, Numerical study of the effect of blowing angle on cooling effectiveness of an effusion cooling, in: ASME TurboExpo, Vienna, Austria, June 14-17, 2004, GT2004-54043.

[21] D. Brauckman, J. von Wolfersdorf, Influence of compound angle on adiabatic film cooling effectiveness and heat transfer coefficient for a row of shaped film cooling holes, in: ASME TurboExpo, Reno-Tahoe, Nevada, USA, June 6-9, 2005, GT2005-68036.

[22] V. Aga, M. Mansour, R.S. Abhari, Aerothermal performance of streamwise and compound angled pulsating film cooling jets, Journal of Turbomachinery 131 (4) (2009) 041015.

[23] M.S. Kavsaoglou, J.A. Schetz, Effects of swirl and high turbulence on a jet in a crossflow, Journal of Aircraft 26 (6) (1989) 539-546.

[24] D.S. Liscinsky, B. True, J.D. Holdeman, Effects of initial conditions on a single jet in crossflow, Report No. NASA TM-107002, AIAA-95-2998, 1995.

[25] C.E. Niederhaus, F.H. Champange, J.W. Jacobs, Scalar transport in a swirling transverse jet, AIAA Journal 35 (11) (1997) 1697-1704.

[26] T. Yingjaroen, A. Pimpin, A. Bunyajitradula, Evolution of mixing regions in jet and swirling jet in crossflow: An experimental study, in: 20th Conference of Mechanical Engineering Network of Thailand, Oct. 18-20, 2006, Nakhon Ratcasima.

[27] H. Yoshizako, K. Yoshiba, I. Akiyama, Diffusion of a jet injected perpendicularly into uniform crossflow, Trans. of Japan Society of Mechanical Engineers A 57 (1991) 354-359.

[28] D.K. Kraus, A.D. Culter, Mixing of swirling jets in a supersonic duct flow, Journal of Power and Propulsion 12 (1) (1995) 170-177.

[29] A.D. Culter, S.E. Doerner, Effects of swirl and skew upon supersonic wall jet in crossflow, Journal of Power and Propulsion 17 (6) (2001) 1327-1332.

[30] A. Bunyajitradulya, S. Sathapornnanon, Sensitivity to tab disturbance of the mean flow structure of nonswirling jet and swirling jet in crossflow, Physics of Fluids 17 (2005) 045102-9.

[31] A. Terzis, I. Stylianou, A.I. Kalfas, P. Ott, Heat transfer and performance characteristics of small axial cooling fans with downstream guide vanes, Journal of Thermal Science 21 (2) (2012) 1-10.

[32] A. Amer, B.A. Jubran, A. Bassam, A.M. Hamdan, Comparison of different two-equation turbulence models for prediction of film cooling from two rows of holes, Numer. Heat Transfer A 21 (2) (1992) 143-162.

[33] S. Sarkar, T.K. Bose, Comparison of different turbulence models for prediction of slot-film cooling: flow and temperature field, Numer. Heat Transfer B 28 (2) (1995) 217-238.

[34] G. Chochua, K.A. Dass, A. Dewan, A computational and experimental investigation of turbulent jet and crossflow interaction, Numer. Heat Transfer A 38 (2000) 557-572.

[35] M. Pathak, K.A. Dass, A. Dewan, An investigation of turbulent rectangular jet discharged into a narrow channel weak crossflow, Journal of Hydrodynamics B 20 (2) (2008) 154-163.

[36] L.L. Yuan, R.L. Street, J.H. Ferziger, Large-eddy simulation of a round jet in crossflow, Journal of Fluid Mechanics 379 (1999) 71-104.

[37] J.U. Schluter, T. Schonfeld, LES of jets in crossflow and its application to a gas turbine burner, Flow Turbulence Combustion 65 (2) (2000) 177-203.

[38] S. Muppidi, K. Mahesh, DNS of round turbulent jets in crossflow, Journal of Fluid Mechanics A574 (2007) 59-84.

[39] F. Muldoon, S. Acharya, DNS study of pulsed film cooling for enhanced cooling effectiveness, Int. Journal of Heat and Mass Transfer 52 (2009) 3118-3127.

[40] S. Acharya, M. Tyagi, A. Hoda, Flow and heat transfer predictions for film-cooling, Annals of New York Academy of Sciences 934 (2001) 110-125.

[41] J.E. Broadwell, R.E. Breidenthal, Structure and mixing of transverse jet in incompressible flow, Journal of Fluid Mechanics 148 (1984) 405-412.

[42] A.R. Karagiozian, An analytical model for the vorticity associated with a transverse jet, AIAA Journal 24 (1986) 429-436.

[43] S.H. Smith, M.G. Mungal, Mixing structure and scaling of the jet in crossflow, Journal of Fluid Mechanics 357 (1998) 83-122.

[44] L. Su, M.G. Mungal, Simultaneous measurements of scalar and velocity field evolution in turbulent crossflowing jets, Journal of Fluid Mechanics 513 (2004) 1-45.